Non-flow correlations and elliptic flow fluctuations in Au + Au collisions at $\sqrt{s_{NN}} = 200$ GeV

B. Alver,[4] B. B. Back,[1] M. D. Baker,[2] M. Ballintijn,[4] D. S. Barton,[2] R. R. Betts,[6] A. A. Bickley,[7] R. Bindel,[7] W. Busza,[4] A. Carroll,[2] Z. Chai,[2] M. P. Decowski,[4] E. García,[6] T. Gburek,[3] N. George,[2] K. Gulbrandsen,[4] C. Halliwell,[6] J. Hamblen,[8] M. Hauer,[2] C. Henderson,[4] D. J. Hofman,[6] R. S. Hollis,[6] R. Hołyński,[3] B. Holzman,[2] A. Iordanova,[6] E. Johnson,[8] J. L. Kane,[4] N. Khan,[8] P. Kulinich,[4] C. M. Kuo,[5] W. Li,[4] W. T. Lin,[5] C. Loizides,[4] S. Manly,[8] A. C. Mignerey,[7] R. Nouicer,[2,6] A. Olszewski,[3] R. Pak,[2] C. Reed,[4] C. Roland,[4] G. Roland,[4] J. Sagerer,[6] H. Seals,[2] I. Sedykh,[2] C. E. Smith,[6] M. A. Stankiewicz,[2] P. Steinberg,[2] G. S. F. Stephans,[4] A. Sukhanov,[2] M. B. Tonjes,[7] A. Trzupek,[3] C. Vale,[4] G. J. van Nieuwenhuizen,[4] S. S. Vaurynovich,[4] R. Verdier,[4] G. I. Veres,[4] P. Walters,[8] E. Wenger,[4] F. L. H. Wolfs,[8] B. Wosiek,[3] K. Woźniak,[3] and B. Wysłouch[4]

(PHOBOS Collaboration)

[1]*Physics Division, Argonne National Laboratory, Argonne, Illinois 60439-4843, USA*

[2]*Physics and C-A Departments, Brookhaven National Laboratory, Upton, New York 11973-5000, USA*

[3]*Institute of Nuclear Physics PAN, Kraków, Poland*

[4]*Laboratory for Nuclear Science, Massachusetts Institute of Technology, Cambridge, Massachusetts 02139-4307, USA*

[5]*Department of Physics, National Central University, Chung-Li, Taiwan*

[6]*Department of Physics, University of Illinois at Chicago, Chicago, Illinois 60607-7059, USA*

[7]*Department of Chemistry, University of Maryland, College Park, Maryland 20742, USA*

[8]*Department of Physics and Astronomy, University of Rochester, Rochester, New York 14627, USA*

(Received 2 February 2010; published 31 March 2010)

This article presents results on event-by-event elliptic flow fluctuations in Au + Au collisions at $\sqrt{s_{NN}} =$ 200 GeV, where the contribution from non-flow correlations has been subtracted. An analysis method is introduced to measure non-flow correlations, relying on the assumption that non-flow correlations are most prominent at short ranges ($|\Delta\eta| < 2$). Assuming that non-flow correlations are of the order that is observed in $p + p$ collisions for long-range correlations ($|\Delta\eta| > 2$), relative elliptic flow fluctuations of approximately 30–40% are observed. These results are consistent with predictions based on spatial fluctuations of the participating nucleons in the initial nuclear overlap region. It is found that the long-range non-flow correlations in Au + Au collisions would have to be more than an order of magnitude stronger compared to the $p + p$ data to lead to the observed azimuthal anisotropy fluctuations with no intrinsic elliptic flow fluctuations.

DOI: 10.1103/PhysRevC.81.034915 PACS number(s): 25.75.Ld, 25.75.Gz

I. INTRODUCTION

The characterization of the collective flow of produced particles by their azimuthal anisotropy has proven to be one of the more fruitful probes of the dynamics of heavy ion collisions at the Relativistic Heavy Ion Collider (RHIC). Flow is sensitive to the early stages of the collision and so the study of flow affords unique insights into the properties of the hot and dense matter that is produced, including information about the degree of thermalization and its equation of state [1].

Elliptic flow, quantified by the second coefficient, v_2, of a Fourier decomposition of the azimuthal distribution of observed particles relative to the event-plane angle, has been studied extensively in collisions at RHIC as a function of pseudorapidity, centrality, transverse momentum, center-of-mass energy, and system size [2–7]. A detailed comparison of these results to theoretical models requires a quantitative understanding of the contributions of other many-particle correlations, referred to as "non-flow" and event-by-event elliptic flow fluctuations [8]. In particular, the measurement of event-by-event fluctuations can pose new constraints on the models of the initial state of the collision and its subsequent hydrodynamic evolution [9,10].

Comparison of the elliptic flow measurements in the Au + Au and Cu + Cu systems at RHIC suggests the existence of large fluctuations in the initial geometry of heavy ion collisions [4]. These initial state fluctuations are expected to lead to event-by-event fluctuations in the measured elliptic flow signal. The measurement in Au + Au collisions of dynamic fluctuations in v_2, including contributions from event-by-event elliptic flow fluctuations and non-flow correlations, has yielded results which are consistent with this expectation [11].

Different methods have been proposed to reduce the contribution of non-flow correlations to the elliptic flow measurements [12,13]. However, the application of these methods to the measurement of elliptic flow fluctuations is limited due to the complicated interplay between non-flow correlations and elliptic flow fluctuations [10,12].

Ollitrault *et al.* have suggested estimating the magnitude of non-flow from measurements of correlations in $p + p$ collisions [14]. However, this estimation may not be completely reliable since a richer correlation structure is observed in Au + Au collisions at RHIC in comparison to the $p + p$ system (e.g., Refs. [15–18]). We propose a method to separate flow and non-flow contributions to the second Fourier coefficient of azimuthal particle pair distributions by studying the three-dimensional two-particle correlation function in $(\eta_1, \eta_2, \Delta\phi)$ space. This separation relies on the assumption that non-flow correlations are most prominent in short range ($\Delta\eta \equiv |\eta_1 - \eta_2| < 2$). The presumably small long-range ($|\Delta\eta| > 2$) non-flow

 ©2010 The American Physical Society

correlations are estimated using $p + p$ data, and HIJING and PYTHIA models. Estimation of non-flow correlations using these assumptions allows the subtraction of the contribution of non-flow correlations to the measured dynamic v_2 fluctuations to obtain event-by-event elliptic flow fluctuations.

This article is organized as follows. The experimental data are described in Sec. II. The measurement of the non-flow correlations and the corresponding event-by-event elliptic flow fluctuations are presented in Secs. III and IV. Discussion and conclusions are included in Sec. V. The numerical relation among dynamic v_2 fluctuations, elliptic flow fluctuations, and non-flow correlations is addressed in the Appendix.

II. EXPERIMENTAL DATA

The data presented here for Au + Au collisions at $\sqrt{s_{NN}} =$ 200 GeV were collected during RHIC Run 4 (2004) using the PHOBOS detector [19]. The primary event trigger requires a coincidence between the paddle counters, which are two sets of 16 scintillator detectors located at $3.2 < |\eta| < 4.5$. An online vertex is determined from the time difference between signals in two sets of 10 Cerenkov counters located at $4.4 < |\eta| < 4.9$ to select collisions that are close to the nominal vertex position $z_{vtx} = 0$ along the beam axis.

Offline vertex reconstruction makes use of information from different subdetectors. Two sets of double-layered silicon vertex detectors (VTX) are located below and above the collision point. PHOBOS also has two spectrometer arms in the horizontal plane used for tracking and momentum measurement of charged particles. For events in the selected vertex region, the most accurate z (along the beam) and y (vertical, perpendicular to the beam) positions are obtained from the vertex detector, while the position along x (horizontal, perpendicular to the beam) comes primarily from the spectrometer.

The collision centrality is defined through bins of fractional total inelastic cross section, determined using the energy deposited in the paddle counters. In this article, we report results for 6–45% most central events, for which measured dynamic v_2 fluctuations values are available [11]. About 4 million collision events were selected in this centrality range by requiring that the primary collision vertex falls within $|z_{vtx}| < 6$ cm.

The analysis presented in this article is performed using the reconstructed hits in the large-acceptance PHOBOS octagon silicon array, covering pseudorapidity $-3 < \eta < 3$ over almost the full azimuth. The angular coordinates (η, ϕ) of charged particles are measured using the location of the energy deposited in the single-layer silicon pads of the octagon. After merging of signals in neighboring pads, in cases where a particle travels through more than a single pad, the deposited energy is corrected for the angle of incidence, assuming that the charged particle originated from the primary vertex. Noise and background hits are rejected by placing a lower threshold on the corrected deposited energy. Depending on η, merged hits with less than 50–60% of the energy loss expected for a minimum ionizing particle are rejected [20]. Since the multiplicity array consists of single-layer silicon detectors, there is no p_T, charge, or mass information available for the particles. All charged particles above a low-p_T cutoff of about 7 MeV/c at $\eta = 3$, and 35 MeV/c at $\eta = 0$ (which is the threshold below which a charged pion is stopped by the beryllium beam pipe) are included on equal footing.

III. MEASUREMENT OF NON-FLOW CORRELATIONS

If the only correlations between particles are due to elliptic flow, then the distribution of the azimuthal angular separation between particles ($\Delta\phi \equiv \phi_1 - \phi_2$) is given by $1 + 2V\cos(2\Delta\phi)$, where $V = v_2(\eta_1) \times v_2(\eta_2)$. In general, the second Fourier coefficient of the $\Delta\phi$ distribution has contributions from both flow and non-flow correlations.

Flow and non-flow contributions can be separated with a detailed study of the η and $\Delta\eta$ dependence of the $\Delta\phi$ correlation function. Consider the distribution of $\Delta\phi$ between particles selected from two η windows centered at η_1 and η_2. We define the quantity $v_2^2(\eta_1, \eta_2)$ as the sum of flow and non-flow contributions to the second Fourier coefficient of the normalized $\Delta\phi$ distribution:

$$v_2^2(\eta_1, \eta_2) \equiv \langle\cos(2\Delta\phi)\rangle(\eta_1, \eta_2). \tag{1}$$

The contributions to the second Fourier coefficient of the $\Delta\phi$ distribution can be parameterized as

$$\langle\cos(2\Delta\phi)\rangle = \left\langle v_2^2\right\rangle_{\text{flow}} + \delta, \tag{2}$$

where δ is the contribution of non-flow correlations [21]. Using the fact that elliptic flow leads to a correlation between all particles in the event and creates a signal which only depends on pseudorapidity ($v_2(\eta)$), we can write:

$$v_2^2(\eta_1, \eta_2) = v_2(\eta_1) \times v_2(\eta_2) + \delta(\eta_1, \eta_2). \tag{3}$$

The measurement of non-flow correlations is therefore achieved in two steps, described in the following sections. First we measure the three-dimensional $(\eta_1, \eta_2, \Delta\phi)$ correlation function to obtain $v_2^2(\eta_1, \eta_2)$. Then we separate the observed $v_2^2(\eta_1, \eta_2)$ distribution to its flow and non-flow components.

A. Two-particle correlations analysis

Two particle correlations have been studied extensively in $(\Delta\eta, \Delta\phi)$ space using the PHOBOS detector for various collision systems [16,22]. In this analysis, we extend the same analysis procedure to $(\eta_1, \eta_2, \Delta\phi)$ space.

The inclusive two-particle correlation function in $(\eta_1, \eta_2, \Delta\phi)$ space is defined as follows

$$R_n(\eta_1, \eta_2, \Delta\phi) = \left\langle \frac{\rho_n^{\text{II}}(\eta_1, \eta_2, \Delta\phi)}{\rho^{\text{mixed}}(\eta_1, \eta_2, \Delta\phi)} - 1 \right\rangle, \tag{4}$$

where $\rho_n^{\text{II}}(\eta_1, \eta_2, \Delta\phi)$ (with unit integral in each η_1, η_2 bin) is the foreground pair distribution obtained by taking two particles from the same event and then averaging over all pairs in all events and $\rho^{\text{mixed}}(\eta_1, \eta_2, \Delta\phi)$ (with unit integral in each η_1, η_2 bin) is the mixed-event background distribution constructed by randomly selecting two particles from two different events with similar vertex position and centrality, representing a product of two single-particle distributions. A vertex bin size of 0.2 cm is used in the event mixing.

The high occupancies measured in $A + A$ collisions require us to account for the high probability of multiple particles

hitting a single pad. Furthermore, secondary effects, such as δ electrons, γ conversions, and weak decays, cannot be all rejected directly. Corrections for the high occupancy in the octagon detector and the secondary effects have been applied in the same way as in the previous $\Delta\eta$, $\Delta\phi$ correlation analyses [16,22].

To correct for the effects of occupancy, each hit is assigned a weight while calculating the correlation function. The weight is calculated using the centrality of the event and pseudorapidity of the hit (which determine the likelihood of multiple particles passing through a pad for a given dE/dx value) and the dE/dx information. The details of the occupancy correction can be found in Ref. [16].

To correct for the secondary detector effects in the data, correlation functions were calculated for different Monte Carlo event generators (PYTHIA, HIJING, and a modified PYTHIA in which all intrinsic correlations have been removed) at $\sqrt{s_{NN}} = 200$ GeV both at the generator level for true primary charged hadrons and with the full GEANT detector simulation and reconstruction procedure. The overall correlation structure for the reconstructed Monte Carlo events consists of both intrinsic and secondary correlations and these two sources of correlations were found to be largely independent of each other, i.e., the correlation from secondaries is mostly determined by sensor thickness, detector geometry, known cross sections, and decay kinematics [22].

The final correlation function, $R^{\text{data}}_{n\,\text{final}}(\eta_1, \eta_2, \Delta\phi)$, is calculated from the raw correlation function, $R^{\text{data}}_{n\text{raw}}(\eta_1, \eta_2, \Delta\phi)$ by subtracting the contribution from secondary correlations:

$$R^{\text{data}}_{n\,\text{final}}(\eta_1, \eta_2, \Delta\phi) = R^{\text{data}}_{n\,\text{raw}}(\eta_1, \eta_2, \Delta\phi) - S(\eta_1, \eta_2, \Delta\phi), \tag{5}$$

where the correction factor $S(\eta_1, \eta_2, \Delta\phi)$ is calculated by comparing the generator level correlation function excluding particles outside the PHOBOS detector acceptance, $R^{\text{MC}}_{n\text{pri,acc}}(\eta_1, \eta_2, \Delta\phi)$, to the correlation function obtained with the full GEANT detector simulation and reconstruction procedure, $R^{\text{MC}}_{n\text{sim}}(\eta_1, \eta_2, \Delta\phi)$:

$$S(\eta_1, \eta_2, \Delta\phi) = R^{\text{MC}}_{n\,\text{sim}}(\eta_1, \eta_2, \Delta\phi) - R^{\text{MC}}_{n\,\text{pri,acc}}(\eta_1, \eta_2, \Delta\phi). \tag{6}$$

The correction factor $S(\eta_1, \eta_2, \Delta\phi)$ is calculated separately for each centrality bin using a set of HIJING events with appropriate average multiplicity. More details on the correction factor S and its dependence on $\Delta\eta$ and $\Delta\phi$ can be found in Ref. [22].

The second Fourier coefficient of the normalized $\Delta\phi$ distribution is calculated from the correlation function by a fit in each (η_1, η_2) bin:

$$R^{\text{data}}_{n\,\text{final}}(\eta_1, \eta_2, \Delta\phi) = 2v_2^2(\eta_1, \eta_2)\cos(2\Delta\phi). \tag{7}$$

The value of $v_2^2(\eta_1, \eta_2)$ can also be calculated directly as

$$v_2^2(\eta_1, \eta_2) = \int R^{\text{data}}_{n\,\text{final}}(\eta_1, \eta_2, \Delta\phi)\cos(2\Delta\phi)d\Delta\phi. \tag{8}$$

The two methods of calculating $v_2^2(\eta_1, \eta_2)$ are found to be equivalent within the systematic uncertainties of the measurement. The resulting $v_2^2(\eta_1, \eta_2)$ distribution for 40–45% centrality bin is shown in Fig. 1.

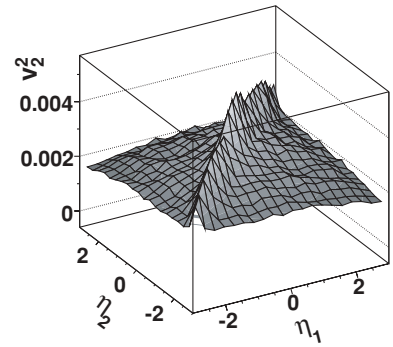

FIG. 1. Second Fourier coefficient of the correlation function $R_n(\Delta\phi, \eta_1, \eta_2)$ as a function of η_1 and η_2 for the 40–45% central Au + Au collisions at $\sqrt{s_{NN}} = 200$ GeV. The ridge along $\eta_1 = \eta_2$ represents the region where non-flow contributions are most prominent.

B. Separation of flow and non-flow contributions

The measured $v_2^2(\eta_1, \eta_2)$ signal in Fig. 1 shows the features expected from Eq. (3): a ridge along $\Delta\eta = 0$ where the non-flow signal is most prominent which sits on a plateau which can be factorized in η_1 and η_2. Assuming non-flow correlations are small at large $\Delta\eta$ separations, it is possible to separate the $v_2^2(\eta_1, \eta_2)$ to its flow and non-flow components.

We start by assuming that non-flow correlations at $|\Delta\eta| > 2$ ($\delta_{|\Delta\eta|>2}$) are zero. Then, we can perform a fit

$$v_2^2(\eta_1, \eta_2) = v_2(\eta_1)^{\text{fit}} \times v_2(\eta_2)^{\text{fit}}; \quad |\eta_1 - \eta_2| > 2, \tag{9}$$

where the fit function $v_2(\eta)^{\text{fit}}$ is an eighth-order even polynomial. The fit in the selected $\Delta\eta$ region can be used to extract the magnitude of correlations due to flow, $v_2(\eta_1)^{\text{fit}} \times v_2(\eta_2)^{\text{fit}}$, in the whole pseudorapidity acceptance. Subtracting the correlations due to flow, we can extract the contribution of non-flow correlations:

$$\delta(\eta_1, \eta_2) = v_2^2(\eta_1, \eta_2) - v_2(\eta_1)^{\text{fit}} \times v_2(\eta_2)^{\text{fit}}. \tag{10}$$

The two components of the $v_2^2(\eta_1, \eta_2)$ distribution in Fig. 1 are shown in Fig. 2.

Different flow measurements with different methods and pseudorapidity acceptances are influenced differently by the non-flow correlation signal. To calculate the effects of non-flow correlation on the measurement of dynamic v_2 fluctuations performed by PHOBOS [11], we calculate the average of the $\delta(\eta_1, \eta_2)$ and $v_2^2(\eta_1, \eta_2)$ distributions over all particle pairs:

$$\langle\delta\rangle = \frac{\int \delta(\eta_1, \eta_2)\frac{dN}{d\eta_1}\frac{dN}{d\eta_2}d\eta_1 d\eta_2}{\int \frac{dN}{d\eta_1}\frac{dN}{d\eta_2}d\eta_1 d\eta_2} \tag{11}$$

$$\langle v_2^2\rangle = \frac{\int v_2^2(\eta_1, \eta_2)\frac{dN}{d\eta_1}\frac{dN}{d\eta_2}d\eta_1 d\eta_2}{\int \frac{dN}{d\eta_1}\frac{dN}{d\eta_2}d\eta_1 d\eta_2}, \tag{12}$$

where $dN/d\eta$ is the observed charged-particle pseudorapidity distribution in the PHOBOS detector. To cancel scale

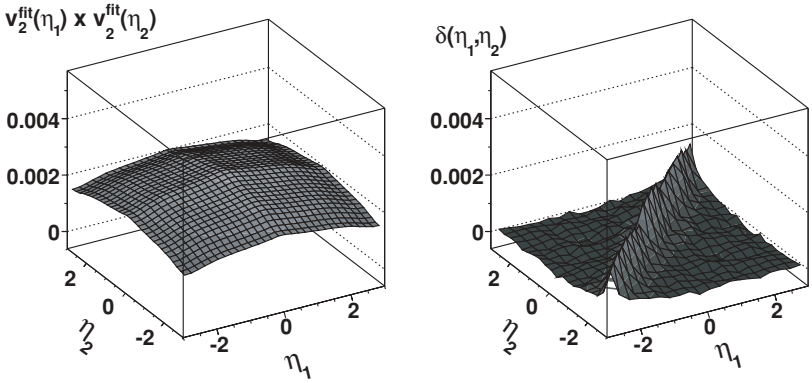

FIG. 2. Flow (left) and non-flow (right) components of $v_2^2(\eta_1, \eta_2)$ in Fig. 1 obtained by Eqs. (9) and (10) assuming non-flow correlations at $|\Delta\eta| > 2$ are negligible.

uncertainties in these quantities, we calculate the "non-flow ratio" given by $\langle\delta\rangle/\langle v_2^2\rangle$.

The systematic uncertainty has been evaluated for the various stages of the non-flow ratio calculation, including the calculation of the correlation function and the fit to $v_2^2(\eta_1, \eta_2)$ to obtain the non-flow ratio. A "digital" occupancy correction with only the event-by-event hit density distribution and no dE/dx information has been used. Hits on the PHOBOS vertex detector, which has a different granularity from the octagon detector have been added to the analysis. Monte Carlo samples with different average multiplicity from the data have been used in the correction procedure. The $\Delta\eta$ cut used in the fit has been varied between 1.2 and 2.7.[1] Different fit functions $v_2(\eta)^{\text{fit}}$ have been used from second-order up to eighth-order polynomials. Finally, the complete analysis chain has been performed by dividing the data set into 6×2-cm-wide vertex bins. Systematic errors are estimated for different steps in the analysis using the variation in the results with respect to the baseline due to these changes in the analysis. The errors in the different steps are added in quadrature to obtain the 90% confidence interval on the measurement of non-flow ratio.

So far, we have assumed that long-range ($|\Delta\eta| > 2$) non-flow correlations can be neglected. However, studies of the correlation function in $p + p$ collisions show that non-flow correlations do extend out to $|\Delta\eta| > 2$ in elementary collisions [22]. Furthermore, a rich correlation structure in high p_T-triggered correlations that extend out to $|\Delta\eta| > 2$ has been observed in 200 GeV Au + Au collision at RHIC [18] after the estimated flow signal is subtracted. However, due to the inherent uncertainty in the flow subtraction, it is not possible to determine the second Fourier coefficient of this correlation structure precisely.

The study of the non-flow ratio as a function of the $\Delta\eta$ cut ($\Delta\eta_c$) for the $v_2(\eta)^{\text{fit}}$ fit carries important information on the magnitude of non-flow at large $\Delta\eta$ separations. If non-flow correlations are short ranged, we expect that the fits should yield non-flow ratio results that saturate for large values of $\Delta\eta_c$. The extracted value of $\langle\delta\rangle/\langle v_2^2\rangle$ is plotted as a function of the $\Delta\eta_c$, where it is assumed that δ is zero for $|\Delta\eta| > \Delta\eta_c$, for different centrality bins in Fig. 3. The saturation expected if non-flow correlations are short range is indeed observed. However, it should be noted that the same saturation pattern could also be observed with a finite magnitude of non-flow that has little $\Delta\eta$ dependence in the region $\Delta\eta > 1.2$.

[1]The octagon detector with a pseudorapidity coverage of $-3 < \eta < 3$ allows particle pairs to be studied up to $\Delta\eta = 6$. However, in this study the $\Delta\eta$ cut is constrained to $\Delta\eta_c < 3$ such that particles from all η values contribute in the fit to obtain $v_2(\eta)$.

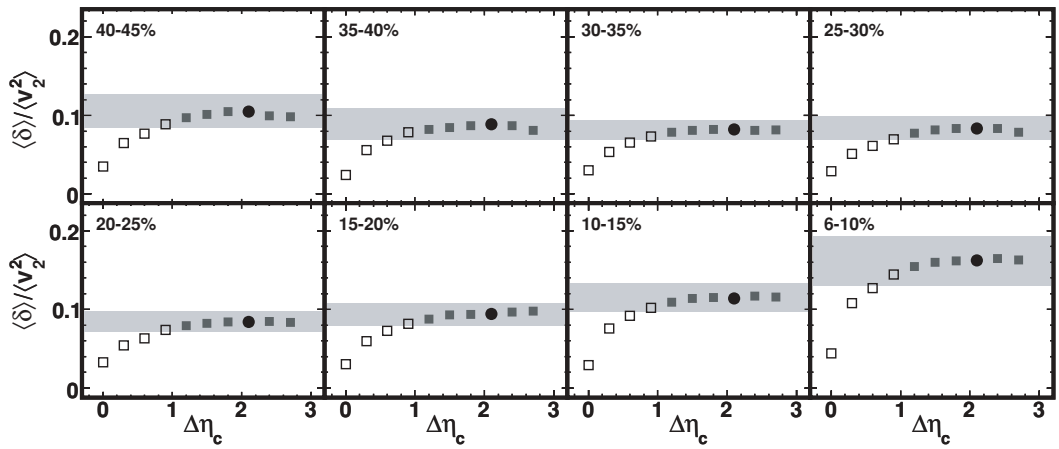

FIG. 3. Measured value of the non-flow ratio ($\langle\delta\rangle/\langle v_2^2\rangle$) as a function of the $\Delta\eta$ cut ($\Delta\eta_c$) where non-flow correlations are assumed to be zero for $|\Delta\eta| > \Delta\eta_c$ for different centrality bins. The black circles (one for each panel) show values for $\Delta\eta_c = 2.1$ with the gray band denoting the 90% C.L. systematic errors on those results as described in the text. The gray squares show values for $1.2 \leqslant \Delta\eta_c \leqslant 2.7$, which are used in the systematic error estimation. Open squares show values for $\Delta\eta_c < 1$.

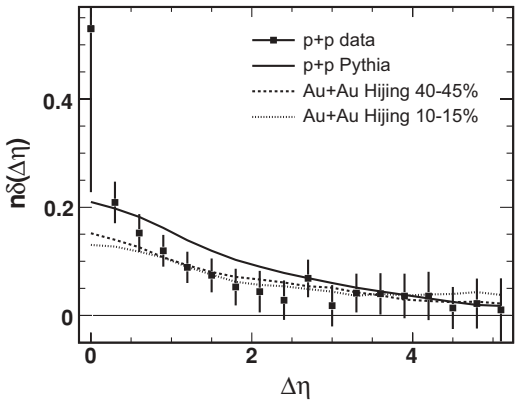

FIG. 4. The magnitude of non-flow correlations (δ) scaled by the charged particle multiplicity (n) in the pseudorapidity range $|\eta| < 3$ as a function of particle pair pseudorapidity separations ($\Delta\eta$) for $p + p$ data and different Monte Carlo generators with no flow correlations at $\sqrt{s_{NN}} = 200$ GeV. The results for $p + p$ data (squares) with 90% C.L. systematic errors are obtained from two particle $\Delta\eta$, $\Delta\phi$ correlations [22]. Statistical errors are not shown.

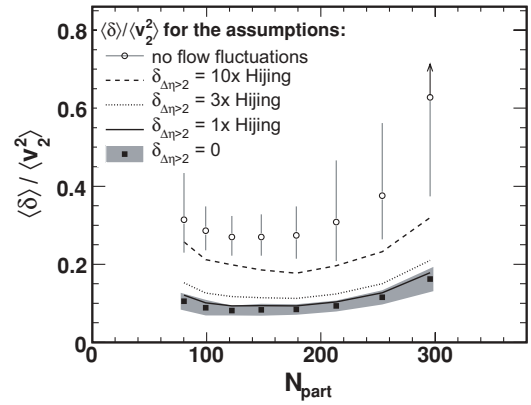

FIG. 5. The non-flow ratio ($\langle\delta\rangle/\langle v_2^2\rangle$) in the PHOBOS octagon detector acceptance as a function of number of participating nucleons ($N_{\rm part}$) in Au + Au collisions at $\sqrt{s_{NN}} = 200$ GeV. The black squares show the results with the assumption that non-flow correlations are negligible at $|\Delta\eta| > 2$. The shaded band shows the 90% confidence systematic errors. The lines show different assumptions about non-flow at $|\Delta\eta| > 2$. The open circles with 90% C.L. systematic errors, show the upper limit on $\langle\delta\rangle/\langle v_2^2\rangle$ obtained by assuming that the measured dynamic fluctuations in v_2 are due to non-flow alone.

To quantitatively assess the effect of nonzero non-flow correlations at large $\Delta\eta$ separations, we analyze the correlation functions obtained from Monte Carlo event generators. In $p + p$ collisions, the magnitude of non-flow correlations, δ, can be directly calculated as the second Fourier coefficient of $\Delta\phi$ correlations since elliptic flow is not present [22]. If $A + A$ collisions were a superposition of $p + p$ collisions, the value of δ would be diluted due to the presence of uncorrelated particles. To compare the strength of non-flow correlations in HIJING (Au + Au) and PYTHIA ($p + p$) models and $p + p$ collisions, we calculate the value of δ scaled by the average event multiplicity, shown in Fig. 4.[2] Both models are observed to roughly reproduce the strength of non-flow correlations in $p + p$ collisions at large $\Delta\eta$. Due to large systematic uncertainties in the $p + p$ data, HIJING simulations are used to model the long range non-flow correlations in Au + Au collisions by assuming non-flow correlations in data are some multiplicative factor, m, times the non-flow in HIJING ($\delta_{\rm MC}(\eta_1, \eta_2)$) for $|\Delta\eta| > 2$. This can be incorporated by modifying Eq. (9):

$$v_2^2(\eta_1, \eta_2) - m\delta_{\rm MC}(\eta_1, \eta_2) = v_2(\eta_1)^{\rm fit} \times v_2(\eta_2)^{\rm fit}; \quad |\Delta\eta| > 2. \tag{13}$$

The resulting non-flow ratio, $\langle\delta\rangle/\langle v_2^2\rangle$, found by applying Eqs. (10)–(12) with the modified $v_2(\eta)^{\rm fit}$ results, is plotted as a function of centrality in Fig. 5 for different assumptions on the magnitude of non-flow at $|\Delta\eta| > 2$. If non-flow correlations are assumed to be present only in $|\Delta\eta| < 2$ ($m = 0$), it is found that they account for approximately 10% of the observed v_2^2 signal averaged over $|\eta| < 3$. The results do not change significantly if the long range non-flow correlations ($\delta_{|\Delta\eta|>2}$) are taken to be the same as the correlations in HIJING ($m = 1$ instead of $m = 0$).

[2]The large uncertainty in the $p + p$ data at $\Delta\eta = 0$ is due to δ electrons and γ conversions, which may not be completely described by GEANT simulations [22].

The upper limit on the non-flow ratio, also shown in Fig. 5, is drawn from the measurement of dynamic v_2 fluctuations [11] assuming that the observed fluctuations are all due to non-flow correlations. The calculation of this limit is described in the Appendix. This limit corresponds to non-flow correlations in Au + Au collisions that are more than an order of magnitude higher than the expected correlations from $p + p$ collisions for $|\Delta\eta| > 2$ ($m > 10$).

IV. ELLIPTIC FLOW FLUCTUATIONS

An event-by-event measurement of the anisotropy in heavy ion collisions yields fluctuations from three sources: statistical fluctuations due to the finite number of particles observed, elliptic flow fluctuations and non-flow correlations. We have previously measured the dynamic fluctuations in v_2 by taking out the statistical fluctuations with a study of the measurement response to the input v_2 signal [11]. The new results on the magnitude of non-flow correlations presented in the previous section can be used to decouple the contributions of genuine elliptic flow fluctuations and non-flow correlations to the measured dynamic fluctuations.

Let us denote the observed distribution of the event-by-event anisotropy as $g(v_2^{\rm obs})$, the distribution of the intrinsic elliptic flow value as $f(v_2)$ and the expected distribution of $v_2^{\rm obs}$ for a fixed value of v_2 as $K(v_2^{\rm obs}, v_2)$. We assume $f(v_2)$ to be a Gaussian in the range $v_2 > 0$ with two parameters, mean ($\langle v_2\rangle$) and standard deviation (σ). The dynamic fluctuations in v_2, can be calculated by unfolding the experimental measurement $g^{\rm exp}(v_2^{\rm obs})$ with a response function $K_n^{\rm exp}(v_2^{\rm obs}, v_2)$ which accounts for detector effects and statistical fluctuations:

$$g^{\rm exp}\left(v_2^{\rm obs}\right) = \int_0^1 K_n^{\rm exp}\left(v_2^{\rm obs}, v_2\right) f_{\rm dyn}(v_2) dv_2. \tag{14}$$

The calculation of intrinsic flow fluctuations ($f_{\rm flow}(v_2)$) from measured dynamic fluctuations ($f_{\rm dyn}(v_2)$) can be summarized

by the following equation:

$$\int_0^1 K_n\left(v_2^{\rm obs}, v_2\right) f_{\rm dyn}(v_2) dv_2 = \int_0^1 K_{n,\delta}\left(v_2^{\rm obs}, v_2\right) f_{\rm flow}(v_2) dv_2, \tag{15}$$

where $K_n(v_2^{\rm obs}, v_2)$ and $K_{n,\delta}(v_2^{\rm obs}, v_2)$ are the response functions for an ideal detector with and without non-flow correlations, respectively. Equation (15) gives the distribution of observed anisotropy for an ideal detector $g(v_2^{\rm obs})$, such that, on the left-hand side, the non-flow correlations are encoded in the dynamic v_2 fluctuations and, on the right-hand side, they are accounted for in the response function $K_{n,\delta}(v_2^{\rm obs}, v_2)$. The response functions $K_n(v_2^{\rm obs}, v_2)$ and $K_{n,\delta}(v_2^{\rm obs}, v_2)$ are given by a Bessel-Gaussian distribution [23] defined as

$$\mathrm{BG}\left(v_2^{\rm obs}; v_2, \sigma_s\right) \equiv \frac{v_2^{\rm obs}}{\sigma_s^2} \exp\left(-\frac{\left(v_2^{\rm obs}\right)^2 + v_2^2}{2\sigma_s^2}\right) I_0\left(\frac{v_2^{\rm obs} v_2}{\sigma_s^2}\right), \tag{16}$$

where I_0 is the modified Bessel function. The fluctuation term σ_s in the response function is a quadratic sum of statistical fluctuations ($\sigma_n = 1/\sqrt{2n}$) due to finite number of particles (n) observed in the detector and a contribution from non-flow correlations ($\sigma_\delta = \sqrt{\delta/2}$).

Equation (15) cannot be simplified analytically. However, it can be solved numerically to calculate relative elliptic flow fluctuations ($\sigma_{\rm flow}/\langle v_2\rangle_{\rm flow}$) that correspond to the measured dynamic v_2 fluctuations ($\sigma_{\rm dyn}/\langle v_2\rangle$) and the non-flow ratio ($\langle\delta\rangle/\langle v_2^2\rangle$) for different assumptions on non-flow at $|\Delta\eta| > 2$. The details of the numerical calculation are given in the Appendix. It has been suggested that the relation between these quantities can be approximated as $\sigma^2_{\rm dyn} = \sigma^2_\delta + \sigma^2_{\rm flow}$ [14]. We have found that this approximation does not hold in the range of our experimental results ($\sigma_{\rm dyn}/\langle v_2\rangle > 0.3$).

The systematic error in the magnitude of relative elliptic flow fluctuations is obtained by propagating the errors in the measured quantities $\sigma_{\rm dyn}/\langle v_2\rangle$ and $\langle\delta\rangle/\langle v_2^2\rangle$ and by varying the procedure to calculate $\sigma_{\rm flow}/\langle v_2\rangle_{\rm flow}$ from these quantities. The errors from different sources are added in quadrature to obtain the 90% confidence interval. The error propagated from the uncertainty in $\sigma_{\rm dyn}/\langle v_2\rangle$ is the dominant contribution to the uncertainty in $\sigma_{\rm flow}/\langle v_2\rangle_{\rm flow}$.

The relative fluctuations in the event-by-event elliptic flow, corrected for contribution of non-flow correlations are presented in Fig. 6 as a function of the number of participating nucleons, in Au + Au collisions at $\sqrt{s_{NN}} = 200$ GeV for 6–45% most central events. The elliptic flow fluctuations are found to be roughly 30–40% if the magnitude of non-flow correlations are assumed to be small for $|\Delta\eta| > 2$. The observed values of relative elliptic flow fluctuations correspond to 87–97% (79–95%) of the previously measured dynamic v_2 fluctuations [11] if non-flow correlations at $|\Delta\eta| > 2$ are assumed to be zero (three times the magnitude in HIJING).

Also shown in Fig. 6 are relative fluctuations in the participant eccentricity obtained from MC Glauber [11] and color glass condensate (CGC) [24] calculations. The measured values of elliptic flow fluctuations are observed to be consistent with both models over the centrality range under study if the long range non-flow correlations are neglected. The same conclusion holds if the long range correlations are assumed to be three times stronger than in $p + p$ collisions, as modeled by HIJING.

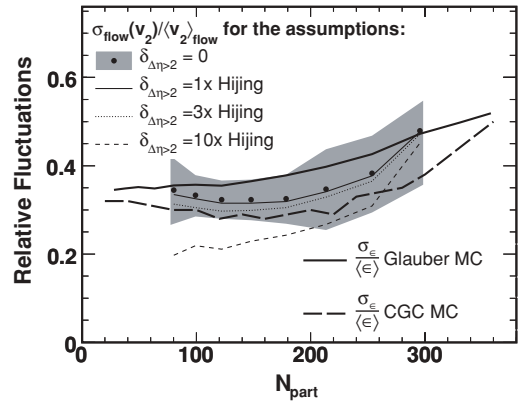

FIG. 6. Relative elliptic flow fluctuations ($\sigma_{\rm flow}/\langle v_2\rangle_{\rm flow}$) as a function of number of participating nucleons ($N_{\rm part}$) in Au + Au collisions at $\sqrt{s_{NN}} = 200$ GeV. The black circles show the results with the assumption that non-flow correlations are negligible at $|\Delta\eta| > 2$. The shaded band shows the 90% confidence systematic errors. The thin lines show results for different assumptions on the magnitude of non-flow at $|\Delta\eta| > 2$. The continuous and dashed thick lines show $\sigma(\epsilon_{\rm part})/\langle\epsilon_{\rm part}\rangle$ values calculated in Glauber MC [11] and CGC [24] models, respectively.

V. SUMMARY AND CONCLUSIONS

We have presented new data on the magnitude of non-flow correlations and the event-by-event elliptic flow fluctuations corrected for non-flow correlations in Au + Au collisions at $\sqrt{s_{NN}} = 200$ GeV. The measurement of non-flow correlations is achieved by utilizing a new correlation analysis with the assumption that non-flow correlations are of the order that is observed in $p + p$ collisions for long-range correlations ($|\Delta\eta| > 2$). The non-flow correlations averaged over the PHOBOS octagon acceptance ($-3 < \eta < 3$) are found to be large, constituting approximately 10% of the measured v_2^2 signal. Studying the dependence of expected azimuthal anisotropy fluctuations due to non-flow correlations, it is found that the long-range non-flow correlations in Au + Au collisions would have to be more than an order of magnitude stronger compared to the $p + p$ data for non-flow correlations to lead to the observed azimuthal anisotropy fluctuations with no intrinsic elliptic flow fluctuations. The method presented in this article can be generally applied in large acceptance detectors to study the contribution of non-flow correlations to the flow signal measured with different approaches.

The magnitude of event-by-event elliptic flow fluctuations were calculated by subtracting the contribution of non-flow correlations to the measured values of dynamic v_2 fluctuations. If the inclusive long-range non-flow correlations in $A + A$ collisions are assumed to be of the order of magnitude that is observed in $p + p$ collisions, the magnitude of event-by-event elliptic flow fluctuations are found to be in agreement with predicted fluctuations of the initial shape of the collision region in both Glauber and CGC models. Therefore these

results support conclusions from previous studies on the importance of geometric fluctuations of the initial collision region postulated to relate elliptic flow measurements in the Cu + Cu and Au + Au systems [4].

ACKNOWLEDGMENTS

This work was partially supported by US DOE Grants DE-AC02-98CH10886, DE-FG02-93ER40802, DE-FG02-94ER40818, DE-FG02-94ER40865, DE-FG02-99ER41099, and DE-AC02-06CH11357; by US NSF Grants 9603486, 0072204, and 0245011; by Polish MNiSW Grant N N202 282234 (2008-2010); by NSC of Taiwan Contract NSC 89-2112-M-008-024; and by Hungarian OTKA Grant (F 049823).

APPENDIX: NUMERICAL CALCULATIONS RELATING MEASURED QUANTITIES TO ELLIPTIC FLOW FLUCTUATIONS

In this section, we describe the numerical calculations performed to relate the measured values of dynamic v_2 fluctuations ($\sigma_{\rm dyn}/\langle v_2\rangle$) and non-flow ratio ($\langle\delta\rangle/\langle v_2^2\rangle$) to intrinsic elliptic flow fluctuations ($\sigma_{\rm flow}/\langle v_2\rangle_{\rm flow}$).

We start by assuming the mean value of the elliptic flow distribution and the magnitude of statistical fluctuations to be given as $\langle v_2\rangle_{\rm flow} = 0.06$ and $\sigma_n = 0.6 \times \langle v_2\rangle_{\rm flow} = 0.036$ [see Eq. (16)]. Then, for given values of $\sigma_{\rm flow}/\langle v_2\rangle_{\rm flow}$ and $\langle\delta\rangle/\langle v_2^2\rangle$, the expected distribution of the observed event-by-event anisotropy $v_2^{\rm obs}$ can be calculated as

$$g\left(v_2^{\rm obs}\right) = \int_0^1 K_{n,\delta}\left(v_2^{\rm obs}, v_2\right) f_{\rm flow}(v_2) dv_2, \tag{A1}$$

where $f_{\rm flow}(v_2)$ is a Gaussian in the range $v_2 > 0$ with mean and standard deviation values given by $\langle v_2\rangle_{\rm flow}$ and $\sigma_{\rm flow}$, respectively, and $K_{n,\delta}(v_2^{\rm obs}, v_2)$ is given by a Bessel-Gaussian [see Eq. (16)],

$$K_{n,\delta}\left(v_2^{\rm obs}, v_2\right) = {\rm BG}\left(v_2^{\rm obs}; v_2, \sigma_s\right). \tag{A2}$$

The fluctuations encoded in the response function $K_{n,\delta}(v_2^{\rm obs}, v_2)$ are given as $\sigma_s^2 = \sigma_n^2 + \sigma_\delta^2$, where σ_δ can be calculated from $\langle v_2\rangle_{\rm flow}$, $\sigma_{\rm flow}$, and $\langle\delta\rangle/\langle v_2^2\rangle$:

$$2\sigma_\delta^2 = \langle\delta\rangle \tag{A3}$$

$$= \langle\delta\rangle \times \frac{\langle v_2\rangle_{\rm flow}^2 + \sigma_{\rm flow}^2}{\langle v_2^2\rangle - \langle\delta\rangle} \tag{A4}$$

$$= \frac{\langle\delta\rangle/\langle v_2^2\rangle}{1 - \langle\delta\rangle/\langle v_2^2\rangle} \times \left(\langle v_2\rangle_{\rm flow}^2 + \sigma_{\rm flow}^2\right). \tag{A5}$$

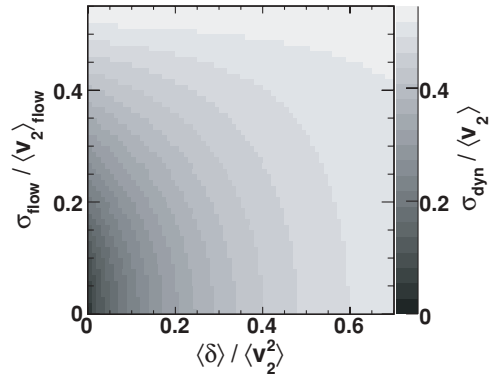

FIG. 7. Dynamic v_2 fluctuations ($\sigma_{\rm dyn}/\langle v_2\rangle$) as a function of elliptic flow fluctuations ($\sigma_{\rm flow}/\langle v_2\rangle_{\rm flow}$) and the non-flow ratio ($\langle\delta\rangle/\langle v_2^2\rangle$) for $\sigma_n/\langle v_2\rangle_{\rm flow} = 0.6$. The observed values of dynamic v_2 fluctuations are roughly given by $\sigma_{\rm dyn}/\langle v_2\rangle \approx 40\%$ [11].

In this derivation, it has been noted that the $\langle v_2^2\rangle$ defined in Eq. (12) includes contributions from flow fluctuations and non-flow correlations.

Next, we calculate the dynamic fluctuations in the measured $v_2^{\rm obs}$ distribution, $g(v_2^{\rm obs})$, by using a response function which incorporates only statistical fluctuations but not non-flow correlations,

$$g\left(v_2^{\rm obs}\right) = \int_0^1 K_n\left(v_2^{\rm obs}, v_2\right) f_{\rm dyn}(v_2) dv_2. \tag{A6}$$

Assuming the dynamic v_2 fluctuations are described by a Gaussian, $f_{\rm dyn}(v_2)$, in the range $v_2 > 0$ with mean and standard deviation values given by $\langle v_2\rangle$ and $\sigma_{\rm dyn}$, the value of $\sigma_{\rm dyn}/\langle v_2\rangle$ can be obtained by fitting Eq. (A6).

The resulting distribution of $\sigma_{\rm dyn}/\langle v_2\rangle$ as a function of $\sigma_{\rm flow}/\langle v_2\rangle_{\rm flow}$ and $\langle\delta\rangle/\langle v_2^2\rangle$ is shown in Fig. 7. The value of $\sigma_{\rm flow}/\langle v_2\rangle_{\rm flow}$ corresponding to measured values of $\sigma_{\rm dyn}/\langle v_2\rangle$ and $\langle\delta\rangle/\langle v_2^2\rangle$ can be extracted from this distribution. Furthermore, the values for $\sigma_{\rm flow}/\langle v_2\rangle_{\rm flow} = 0$ can be used to set an upper limit on the magnitude of the non-flow ratio.

Since the related quantities are given as ratios, the value of $\langle v_2\rangle_{\rm flow}$ set at the beginning is arbitrary. It was observed that $\sigma_n/\langle v_2\rangle$ is roughly given by 0.6 for the dynamic v_2 fluctuations measurement for all centrality bins in the centrality range studied. The calculation was repeated for values of $\sigma_n/\langle v_2\rangle_{\rm flow} = 0.4$ and 0.8. The differences in results, which were found to be small, are incorporated in the systematic errors.

[1] P. F. Kolb, P. Huovinen, U. W. Heinz, and H. Heiselberg, Phys. Lett. B **500**, 232 (2001).

[2] B. B. Back *et al.* (PHOBOS Collaboration), Phys. Rev. Lett. **94**, 122303 (2005).

[3] B. B. Back *et al.* (PHOBOS Collaboration), Phys. Rev. C **72**, 051901 (2005).

[4] B. Alver *et al.* (PHOBOS Collaboration), Phys. Rev. Lett. **98**, 242302 (2007).

[5] B. B. Back *et al.* (PHOBOS Collaboration), Nucl. Phys. A **757**, 28 (2005).

[6] J. Adams *et al.* (STAR Collaboration), Nucl. Phys. A **757**, 102 (2005).

[7] K. Adcox *et al.* (PHENIX Collaboration), Nucl. Phys. A **757**, 184 (2005).

[8] H. Song and U. W. Heinz, J. Phys. G **36**, 064033 (2009).

[9] T. Osada, C. E. Aguiar, Y. Hama, and T. Kodama (2001), arXiv:nucl-th/0102011v1.
[10] B. Alver *et al.* (PHOBOS Collaboration), Phys. Rev. C **77**, 014906 (2008).
[11] B. Alver *et al.* (PHOBOS Collaboration) submitted to Phys. Rev. Lett. (2007), arXiv:nucl-ex/0702036v2.
[12] N. Borghini, P. M. Dinh, and J.-Y. Ollitrault, Phys. Rev. C **64**, 054901 (2001).
[13] A. Bilandzic, N. van der Kolk, J.-Y. Ollitrault, and R. Snellings (2008), arXiv:0801.3915v1.
[14] J.-Y. Ollitrault, A. M. Poskanzer, and S. A. Voloshin, Phys. Rev. C **80**, 014904 (2009).
[15] J. Adams *et al.* (STAR Collaboration), Phys. Rev. C **73**, 064907 (2006).
[16] B. Alver *et al.* (PHOBOS Collaboration), Phys. Rev. C **81**, 024904 (2010).
[17] B. I. Abelev *et al.* (STAR Collaboration), Phys. Rev. C **80**, 064912 (2009).
[18] B. Alver *et al.* (PHOBOS Collaboration), Phys. Rev. Lett. **104**, 062301 (2010).
[19] B. B. Back *et al.* (PHOBOS Collaboration), Nucl. Instrum. Methods A **499**, 603 (2003).
[20] B. B. Back *et al.* (PHOBOS Collaboration), Phys. Rev. Lett. **87**, 102303 (2001).
[21] A. M. Poskanzer and S. A. Voloshin, Phys. Rev. C **58**, 1671 (1998).
[22] B. Alver *et al.* (PHOBOS Collaboration), Phys. Rev. C **75**, 054913 (2007).
[23] J.-Y. Ollitrault, Phys. Rev. D **46**, 229 (1992).
[24] H.-J. Drescher and Y. Nara, Phys. Rev. C **76**, 041903(R) (2007).